A&A 565, A116 (2014)
DOI: 10.1051/0004-6361/201323351

Astronomy & Astrophysics

Fossil group origins

IV. Characterization of the sample and observational properties of fossil systems

S. Zarattini[1,2,3], R. Barrena[1,2], M. Girardi[4,5], N. Castro-Rodriguez[1,2], W. Boschin[6], J. A. L. Aguerri[1,2], J. Méndez-Abreu[1,2,18], R. Sánchez-Janssen[7], C. Catalán-Torrecilla[8], E. M. Corsini[3,9], C. del Burgo[10], E. D'Onghia[11,12], N. Herrera-Ruiz[13], J. Iglesias-Páramo[14,15], E. Jimenez Bailon[16], M. Lozada Muoz[16], N. Napolitano[17], and J. M. Vilchez[14]

[1] Instituto de Astrofísica de Canarias, calle vía Láctea s/n, 38205 La Laguna, Tenerife, Spain
e-mail: stefano@iac.es
[2] Universidad de La Laguna, Dept. Astrofísica, 38206 La Laguna, Tenerife, Spain
[3] Dipartimento di Fisica e Astronomia "G. Galilei", Università degli Studi di Padova, vicolo dell'Osservatorio 3, 35122 Padova, Italy
[4] Dipartimento di Fisica-Sezione Astronomia, Università degli Studi di Trieste, via Tiepolo 11, 34143 Trieste, Italy
[5] INAF – Osservatorio Astronomico di Trieste, via Tiepolo 11, 34143 Trieste, Italy
[6] Fundación Galileo Galilei – INAF, Rambla José Ana Fernández Pérez 7, 38712 Breña Baja, La Palma, Spain
[7] NRC Herzberg Institute of Astrophysics, 5071 West Saanich Road, Victoria V9E 2E7, Canada
[8] Departamento de Astrofísica y CC. de la Atmósfera, Universidad Complutense de Madrid, 28040 Madrid, Spain
[9] INAF – Osservatorio Astronomico di Padova, vicolo dell'Osservatorio 5, 35122 Padova, Italy
[10] Instituto Nacional de Astrofísica, Óptica y Electrónica, Luis Enrique Erro 1, Sta. Ma. Tonantzintla, Puebla, México
[11] Astronomy Department, University of Wisconsin, 475 Charter St., Madison WI 53706, USA
[12] Alfred P. Sloan Fellow
[13] Astronomisches Institut der Universität Bochum, Universitätsstr. 150, 44801 Bochum, Germany
[14] Instituto de Astrofísica de Andalucía – C.S.I.C., 18008 Granada, Spain
[15] Centro Astronómico Hispano Alemán, C/ Jesús Durbán Remón 2-2. 04004 Almería, Spain
[16] Instituto de Astronomía Apdo. 70-264, Cd. Universitaria, México DF 04510 México
[17] INAF – Osservatorio Astronomico di Capodimonte, Salita Moiariello 16, 80131 Napoli, Italy
[18] School of Physics and Astronomy, University of St Andrews, North Haugh, St Andrews KY16 9SS, UK

Received 28 December 2013 / Accepted 26 February 2014

ABSTRACT

Context. Virialized halos grow by the accretion of smaller ones in the cold dark matter scenario. The rate of accretion depends on the different properties of the host halo. Those halos for which this accretion rate was very fast and efficient resulted in systems dominated by a central galaxy surrounded by smaller galaxies that were at least two magnitudes fainter. These galaxy systems are called fossil systems, and they can be the fossil relics of ancient galaxy structures.
Aims. We started an extensive observational program to characterize a sample of 34 fossil group candidates spanning a broad range of physical properties.
Methods. Deep r-band images were obtained with the 2.5-m *Isaac Newton* Telescope and Nordic Optic Telescope. Optical spectroscopic observations were performed at the 3.5-m Telescopio Nazionale *Galileo* for ∼1200 galaxies. This new dataset was completed with Sloan Digital Sky Survey Data Release 7 archival data to obtain robust cluster membership and global properties of each fossil group candidate. For each system, we recomputed the magnitude gaps between the two brightest galaxies (Δm_{12}) and the first and fourth ranked galaxies (Δm_{14}) within 0.5 R_{200}. We consider fossil systems to be those with $\Delta m_{12} \geq 2$ mag or $\Delta m_{14} \geq 2.5$ mag within the errors.
Results. We find that 15 candidates turned out to be fossil systems. Their observational properties agree with those of non-fossil systems. Both follow the same correlations, but the fossil systems are always extreme cases. In particular, they host the brightest central galaxies, and the fraction of total galaxy light enclosed in the brightest group galaxy is larger in fossil than in non-fossil systems. Finally, we confirm the existence of genuine fossil clusters.
Conclusions. Combining our results with others in the literature, we favor the merging scenario in which fossil systems formed from mergers of L^* galaxies. The large magnitude gap is a consequence of the extreme merger ratio within fossil systems and therefore it is an evolutionary effect. Moreover, we suggest that at least one fossil group candidate in our sample could represent a transitional fossil stage. This system could have been a fossil in the past, but not now owing to the recent accretion of another group of galaxies.

Key words. galaxies: formation – galaxies: groups: general – galaxies: clusters: general – galaxies: elliptical and lenticular, cD – galaxies: evolution – galaxies: distances and redshifts

1. Introduction

Fossil systems are group- or cluster-sized objects whose luminosity is dominated by a very massive central galaxy (Mendes de Oliveira et al. 2006; Cypriano et al. 2006). In the current cold dark matter (CDM) scenario, these objects formed hierarchically at an early epoch of the Universe and then slowly evolved until the present day. That is why they are called *fossils*.

The study of this particular kind of object started two decades ago, when Ponman et al. (1994) suggested that RX-J1340.6+4018 was probably the remains of an ancient group of galaxies. Later, Jones et al. (2003) gave the first observational definition of fossil groups (FGs) as systems characterized by a magnitude gap larger than 2 mag in the r-band between the two brightest galaxies of the system within half the virial radius. Moreover, the central galaxy should be surrounded by a diffuse X-ray halo, with a luminosity of at least $L_X > 10^{42}\ h_{50}^{-2}$ erg s^{-1}, with the aim of excluding bright isolated galaxies.

Many optical and X-ray observational properties of FGs have been studied, but always on small samples or individual systems. These properties can be grouped in (i) properties of the intracluster hot component; (ii) properties of the galaxy population; and (iii) properties of the brightest group galaxy (hereafter BGG). Referring to the hot gas component, fossil and non-fossil systems generally show a similar L_X–T_X relation (see Khosroshahi et al. 2007; Harrison et al. 2012). Differences in scaling relations that combine both optical and X-ray properties were detected. In particular, some authors found different relations in optical vs. X-ray luminosity (L_{opt}–L_X), X-ray luminosity vs. velocity dispersion of the clusters galaxies (L_X–σ_v), and X-ray temperature vs. velocity dispersion (T_X–σ_v). In these works, for any given L_{opt}, FGs are more luminous and hotter in the X-rays than normal groups or clusters. These differences were interpreted as a deficit formation of L^* galaxies in FGs (see Proctor et al. 2011). In contrast, other authors such as Voevodkin et al. (2010) and Harrison et al. (2012) did not find any different relation between X-ray and optical quantities for FGs and normal groups and clusters. They claimed that the previous differences were due to observational biases in the selection of FGs or inhomogeneity between the FGs and the comparison sample. In addition, high signal-to-noise ratio (S/N) and high resolution X-ray observations of fossil systems seem to confirm that fossil systems are formed inside high centrally concentrated dark matter (DM) halos (Sun et al. 2004; Khosroshahi et al. 2006), with large mass-to-light ratios, which could indicate an early formation. Nevertheless, most of the fossil systems do not show cooling cores (but see also Démoclès et al. 2010) as normal clusters, suggesting that strong heating mechanisms, such as AGN feedback or cluster mergers, could heat the central regions of their DM halos (Sun et al. 2004; Khosroshahi et al. 2004, 2006; Mendes de Oliveira et al. 2009).

The galaxy luminosity function (hereafter LF) is a powerful tool for studying the galaxy population in clusters. In the past, several works investigated the galaxy LF in fossil systems. They found that the LF of these objects are well fitted by single Schechter function, but there is a large variety of values in the faint-end slope (α) of the LFs of FGs. In particular, the values of α measured goes from -1.6 to -0.6 (see Cypriano et al. 2006; Khosroshahi et al. 2006; Mendes de Oliveira et al. 2006, 2009; Zibetti et al. 2009; Aguerri et al. 2011; Lieder et al. 2013). Unfortunately, all these studies were performed on single FGs or very small samples, and a systematic study of LFs of statistically meaningful samples of FGs remains to be done.

The brightest central galaxies of fossil systems are among the most massive and luminous galaxies known in the Universe. In fact, the luminosity and the fraction of light contained in the BGGs correlate with the magnitude gap (Harrison et al. 2012). Some observations (Khosroshahi et al. 2006) show that these objects are different from both isolated elliptical galaxies and central galaxies in non-fossil clusters in the sense that they have disky isophotes in the center and their luminosity correlates with velocity dispersion, while other authors (La Barbera et al. 2009; Méndez-Abreu et al. 2012) found no differences in isophotal shapes between fossil and non-fossil central galaxies. In Méndez-Abreu et al. (2012) we analyzed deep K-band images of 20 BGGs in fossil and non-fossil systems and showed that these galaxies follow the tilted fundamental plane of normal ellipticals (see Bernardi et al. 2011). This suggests that BGGs are dynamically relaxed systems that suffer dissipational mergers during their formation. On the other hand, they depart from both Faber-Jackson and luminosity-size relations. In particular, BGGs have larger effective radii and smaller velocity dispersions than those predicted by these relations. We infer that BGGs grew throughout dissipational mergers in an early stage of their evolution and then assembled the bulk of their mass through subsequent dry mergers. Nevertheless, stellar population studies of BGGs in fossil systems suggest that their age, metallicity, and α-enhancement are similar to those of bright ellipticals field galaxies (see La Barbera et al. 2009; Eigenthaler & Zeilinger 2013).

In numerical simulations, FGs are found to be a particular case of structure formation. They are supposed to be located in highly concentrated DM halos, so that they can assemble half of their DM mass at $z > 1$. Then, the FGs grow via minor mergers alone, and only accrete about one galaxy from $z \approx 1$ down to the present time, while regular groups accrete about three galaxies in the same range of time (von Benda-Beckmann et al. 2008). Dariush et al. (2007) show that the mass assembled at any redshift is higher in fossil than in non-fossil systems. This means that the formation time is, on average, shorter for FGs than for regular systems (D'Onghia et al. 2005; von Benda-Beckmann et al. 2008), leaving FGs enough time to merge L^* galaxies in one very massive central object. In fact, simulations predict that the timescale for merging via dynamical friction is inversely proportional to the mass of the galaxy, thus favoring the merging of larger objects, so dynamical friction would be responsible for the lack of L^* galaxies that is reflected in the requested magnitude gap of the observational definition. Moreover, to enhance the high efficiency in the merging process, FGs should have particular dynamical properties, such as the location of massive satellites on orbits with low angular momentum (see Sommer-Larsen 2006). A combination of high mass satellite and low angular momentum orbits thus boosts the efficiency of the merging process (Boylan-Kolchin et al. 2008). Recently, Lidman et al. (2013) have demonstrated that the growth of the BCGs since $z \sim 1$ is mainly due to major mergers, suggesting that this could be the dominant mechanism in accreting the mass of central galaxies in clusters, thus indirectly supporting the merging scenario for fossil systems, which would differ from regular clusters only for the early time formation.

Nevertheless, the evolutionary picture in which FGs became fossils in the early Universe and then evolved undisturbed is not the only proposed scenario. In the framework of the merging scenario Díaz-Giménez et al. (2008) suggest that first-ranked galaxies in fossil systems have the last major merger later than non-fossil ones. This means that the formation of large magnitude gaps as those in current fossil systems is a long-term process. In addition, von Benda-Beckmann et al. (2008) predict that being a fossil could be a transitional status for some systems. Thus, some

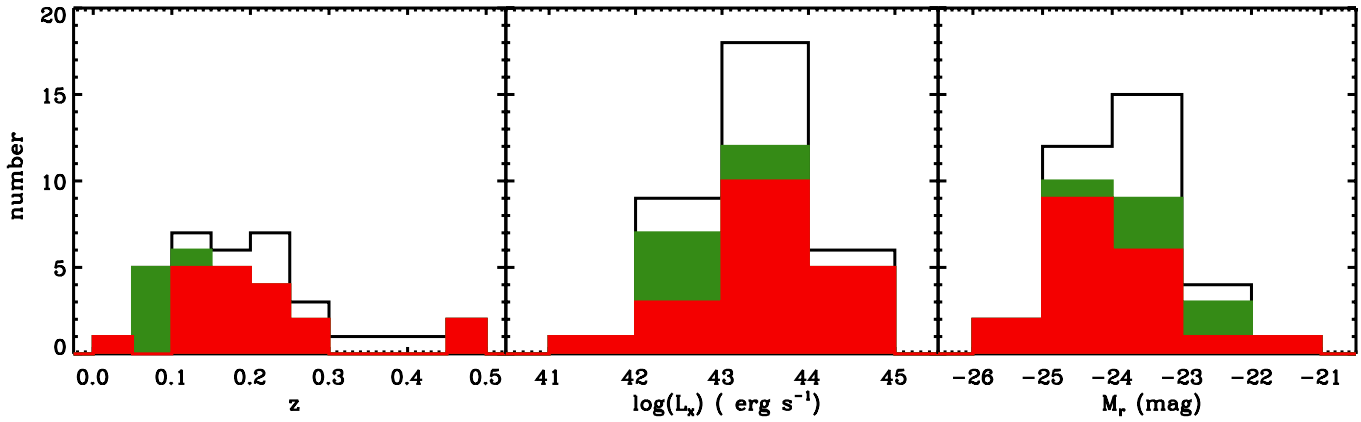

Fig. 1. Distribution of redshifts (*left panel*), X-ray luminosities (*central panel*), and absolute magnitudes of the BGGs (*right panel*) for the sample of 34 FG candidates by Santos et al. (2007) (black line) and for our subsample of 25 FG candidates either with our own (red line) or with SDSS spectroscopy (green line).

fossil systems have become non-fossil ones in recent epochs owing to accretion of nearby galaxy groups.

An alternative formation scenario in which the magnitude gap of the systems appears at the beginning of the formation process can also explain the reported observational properties. This is the so-called monolithic scenario, in which fossil systems formed with a top heavy LF. In this scenario, the magnitude gap is due to a primordial deficient formation of L^* galaxies (Mulchaey & Zabludoff 1999).

All the observational results presented in the literature are limited by how few FGs are known in the literature. A more general study of fossil systems is needed in order to distinguish between these two formation scenarios. For this reason, we started an extensive observational program called fossil group origins (FOGO), aimed at carrying out a large, systematic, and multi-wavelength study of a sample of 34 FGs candidates identified by Santos et al. (2007). The specific goals of the program include mass and dynamics of FGs, properties of their galaxy populations, formation of the central galaxies and their connection with the intragroup medium, properties of the extended diffuse light, and agreement with old and new simulations. The details of the project are summarized in the first paper of the series (Aguerri et al. 2011). The structural properties of the BGGs in fossil and non-fossil systems were shown in the second paper (Méndez-Abreu et al. 2012). The L_X−L_{opt} relations of fossil and normal systems are analyzed in Girardi et al. (2014), the third paper. This is the fourth paper in the series, and it is devoted to characterizing the sample. In particular, we recomputed the magnitude gaps of the systems by using new spectroscopic redshift measurements. These new data provide robust cluster membership and global properties for the systems. Only 15 out of 34 turned out to be fossil systems according to the standard definition (see Jones et al. 2003). We have also analyzed the relations between central galaxies in FGs and non-FGs and other quantities such as magnitude gaps and velocity dispersion of the host halo. FGs follow the same relations as non-FGs, but they are extreme cases.

The paper is organized as follows. The description of the sample is given in Sect. 2. The available dataset is shown in Sect. 3. Radial velocity determination is presented in Sect. 4. The results are given in Sect. 5. Sections 6 and 7 report the discussion and conclusions of the paper, respectively. Unless otherwise stated, we give errors at the 68% confidence level. Throughout this paper, we use $H_0 = 70\,\mathrm{km\,s^{-1}\,Mpc^{-1}}$, $\Omega_\Lambda = 0.7$, and $\Omega_M = 0.3$.

2. Description of the sample

The FOGO sample is based on the Santos et al. (2007) FG candidates selected from the Sloan Digital Sky Survey Data Release 5 (SDSS DR5, Adelman-McCarthy et al. 2007). Santos et al. (2007) selected 112.510 galaxies brighter than $r = 19$ in the luminous red galaxy catalog (LRG, Eisenstein et al. 2001). A cross-match with the Rosat All Sky Survey catalog (RASS, Voges et al. 1999) was performed to look for a diffuse X-ray halo of at least 10^{42} erg s^{-1} and closer than 0.′5 from the position of each LRG. Finally, they looked for the brightest companions of each of the remaining LRGs within a fixed radius of $0.5h_{70}^{-1}$ Mpc to satisfy the magnitude gap $\Delta m_{12} \geq 2$ between the two brightest galaxies of the group. The final catalog comprises 34 FG candidates with some unique characteristics: the sample spans the last 5 Gyr of galaxy evolution ($0 \leq z \leq 0.5$), it has a wide range of X-ray luminosities and therefore masses, and the absolute magnitude of the central BGG covers a wide range ($-25.3 \leq M_r \leq -21.3$).

In this work we present analysis of the 34 systems of the sample of Santos et al. (2007). For each system we were able to compute new Δm_{12} and Δm_{14} gaps by combining our deep r-band images with photometric data from the SDSS DR7. We measured the line-of-sight (LOS) velocity dispersion for those systems with at least ten members within R_{200}[1]. This subsample is formed by 24 groups with redshift obtained mainly from our own spectroscopy (∼1200 new velocities, see Sect. 3.2). In Fig. 1 we show the distribution of redshifts, X-ray luminosities, and absolute magnitude of the 34 BGGs of the sample by Santos et al. (2007) and of our subsample of 24 objects plus FGS28, for which only one member galaxy is found within R_{200}. The Kolmogorov-Smirnov test confirms that our subsample of 25 and the whole sample of 34 FG candidates by Santos et al. (2007) come from the same parent distribution.

Hereafter, we identify each system using the notation FGS + ID, where ID is the identifying number in Table 1 of Santos et al. (2007).

3. The data

3.1. Photometric data

Deep images for 22 of the FG candidates were obtained using the 2.5-m Nordic Optical Telescope (NOT) at the Roque de

[1] The radius R_δ is the radius of a sphere with mass over density δ times the critical density at the redshift of the galaxy system.

los Muchachos Observatory (ORM, La Palma, Spain) in the period between 2008−2011. We used the Andalucía Faint Object Spectrograph and Camera (ALFOSC) in imaging mode with SDSS *r*-band filter. The detector was a CCD of 2048 × 2048 pixels with a plate scale of 0.″19 pixel^{-1}. For ten more candidates, images in the same band were taken at the 2.5-m *Isaac Newton* Telescope (INT) at the ORM in the same period using the Wide Field Camera (WFC). It consists of four 2000 × 4000 CCDs with a scale of 0.″33 pixel^{-1}. All the images were obtained under photometric conditions, and the mean value of the seeing FWHM was 1.″0. Only FGS27 and FGS33 were observed under bad seeing conditions. Their final combined images had a seeing $FWHM \geq 2.''0$ and therefore they were replaced with SDSS images. For FGS09 and FGS26, it was impossible to obtain deep images due to a very bright star located close to their BGGs. SDSS photometric images were also used for these two systems.

Data reduction was performed using standard IRAF[2] routines, correcting for bias and flat field. In most of the cases, after these corrections, we detected some residual light. To achieve the best possible flat field correction, we obtained a super-flat field using a combination of the scientific images. Then we corrected the scientific images once again with such a new super-flat field (see Aguerri et al. 2011, for details). The images were combined and calibrated using SDSS data of the unsaturated stars available in the field of view. The typical root mean square (rms) error of the calibration is 0.08 mag.

3.2. Spectroscopic data

We used the SDSS DR6 (Adelman-McCarthy et al. 2008) photometric redshifts ($z_{\rm phot}$) to select reliable targets for multi-object spectroscopy (MOS). For each FG candidate we downloaded a catalog with all galaxies brighter than $m_r = 22$ within a radius of 30 arcmin around each BGG. The m_r value represents the completeness limit of the photometric catalog of the SDSS, and the selected radius is larger than a virial radius for all our FG candidates. Then, we considered as possible targets only galaxies with photometric redshift within the range of $\Delta z_{\rm phot} \pm 0.15$ from the spectroscopic redshift of the BGG. This value was chosen because the typical error on photometric redshift in the SDSS DR6 is about 0.1. Finally, we visually selected the targets trying to maximize the number of slits per mask. We also put 60 slits on galaxies with spectroscopic redshift in the SDSS DR6 for a comparison. We observed a total of 51 masks with on average 30 slits per mask. We obtained 1227 spectra with a $S/N \geq 5$, which is enough to measure the LOS velocity of the galaxies.

MOS observations were performed under the International Time Program (ITP) of the ORM in the period between 2008 and 2010. Additional observations were done under one Italian and two Spanish Time Allocation Comittee (TAC) runs between 2008 and 2012. The data were taken at the 3.5-m Telescopio Nazionale *Galileo* (TNG) using Device Optimized for the LOw RESolution (DOLORES) in the MOS mode. The instrument has a CCD of 2048 × 2048 pixels with a pixel size of 13.5 μm and a 0.″252 pixel^{-1} scale. We used the LR-B Grism with a dispersion of 187 Å mm^{-1}, together with 1.″6 slits. This led to a final resolution of $R = 365$ in the wavelength range 3000−8430 Å. The typical exposure time was of 3 × 1800 s per mask, and the mean FWHM of the seeing was 1.″0.

We performed the data reduction using standard IRAF procedures. We did not correct for bias and flat field because the uncorrected spectra turn out to be less noisy than the corrected ones. In particular, the measured LOS velocities are the same in both the corrected and uncorrected spectra, but the uncertainties are greater when the bias and flat field corrections are applied. The cosmic ray correction was performed during the combining process of the different exposures we obtained for each mask. The sky was evaluated by measuring the median value in the outer regions of each spectrum. To perform the wavelength calibration, we used two different lamps (Ne+He and Ne+Hg) to have arc lines in both the red and blue parts of the spectrum. The typical uncertainty of the wavelength calibration was <0.1 Å (rms). Finally, we corrected for the instrumental distortions by measuring the [OI]λ5577 Å sky line. This is crucial since we divided each mask exposure into individual exposures of 1800 s, sometimes taken on different days or runs. The mean error associated to the instrumental distortions is 0.85 Å (which corresponds to 45 km s^{-1}), but it can be as large as 8 Å (450 km s^{-1}). We corrected all the measured LOS velocities to take the systematic error due to the instrumental distortions into account.

4. Redshift catalog

4.1. Line of sight velocity measurement

The LOS velocities were measured using the cross-correlation technique (Tonry & Davis 1979) implemented in the IRAF task XCSAO of the package RVSAO[3]. For each spectrum the task performs a cross-correlation with six templates (Kennicutt 1992), corresponding to different types of galaxies (E, S0, Sa, Sb, Sc, Irr). The template with the highest S/N value of the cross-correlation peak was chosen. In addition, we visually inspected all the spectra to verify the velocity determination. In most of the cases, the LOS velocity was obtained from the absorption lines. Nevertheless, in some spectra with low S/N (especially for faint objects with $m_r > 20.5$), the emission lines were measured with the IRAF task EMSAO to obtain the LOS velocity. In Fig. 2 the absorption lines are detectable in the five brightest objects but not in the faintest one. The latter is actually the only galaxy with $m_r > 21$ for which we measured the LOS velocity. The nominal uncertainties given by the cross–correlation algorithm are known to be smaller than the true ones (see, Malumuth et al. 1992; Bardelli et al. 1994; Ellingson & Yee 1994; Quintana et al. 2000). The uncertainties obtained through the RVSAO procedure were multiplied by a factor 2, following previous analyses (Barrena et al. 2009, and references therein) on data acquired with the same instrumental setup and with comparable quality or our own. Moreover, to be conservative, we assumed the largest between the formal uncertainty and 100 km s^{-1} for the LOS velocities measured with the EMSAO procedure. We adopted the weighted mean of the different determinations and the corresponding error for the galaxies with repeated measurements. The rms of this difference for 48 galaxies is 107 km s^{-1}.

4.2. Additional line of sight velocities

To have the most LOS velocities for the 34 FG candidates, we added all available redshifts within R_{200} from the SDSS-DR7. Figure 3 shows the comparison between ours and the SDSS LOS velocity measures for the 60 galaxies for which both values are available. The rms of the difference between the two values

[2] IRAF is distributed by the National Optical Astronomy Observatories, which are operated by the Association of Universities for Research in Astronomy, Inc., under cooperative agreement with the National Science Foundation.

[3] RVSAO was developed at the Smithsonian Astrophysical Observatory Telescope Data Center.

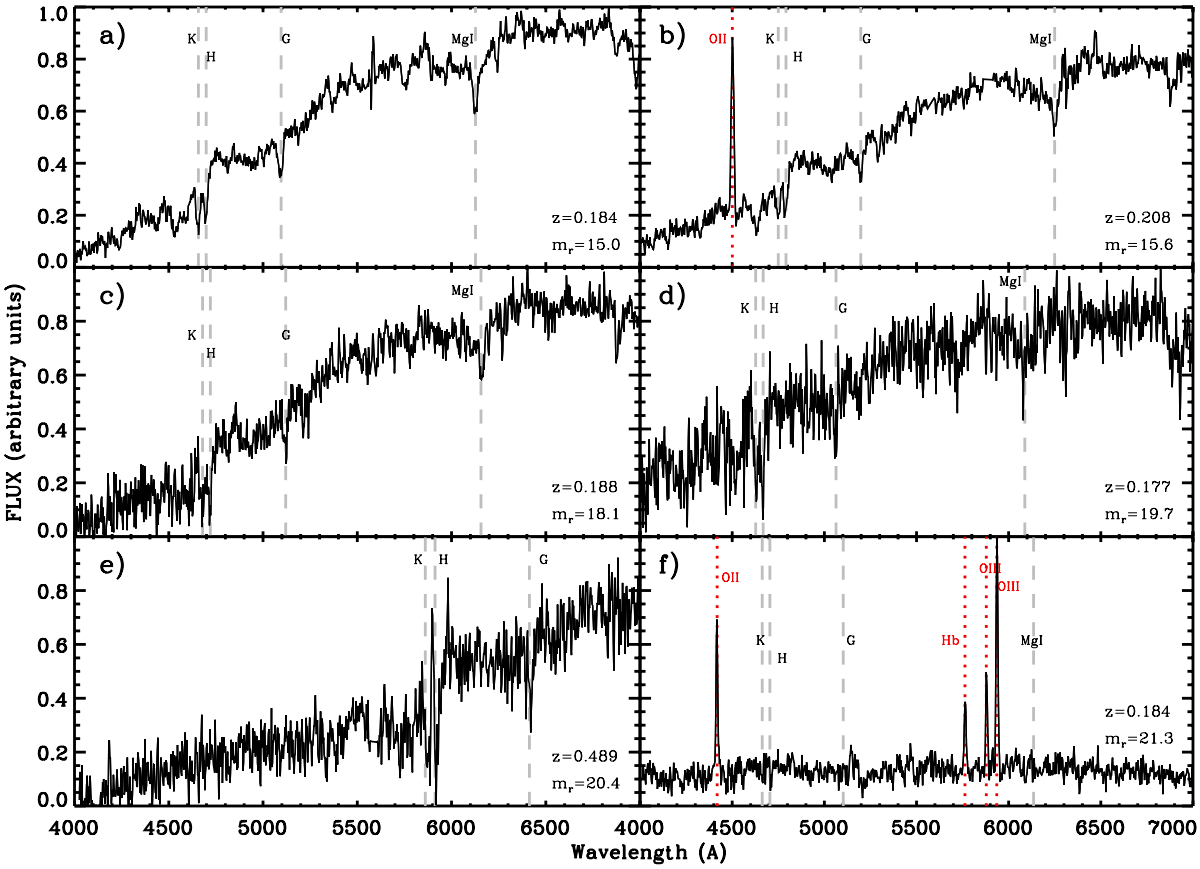

Fig. 2. Examples of spectra with decreasing S/N (from panel **a)** to panel **f)**) from our dataset. The main absorption and emission lines are marked with dashed gray and dotted red lines, respectively.

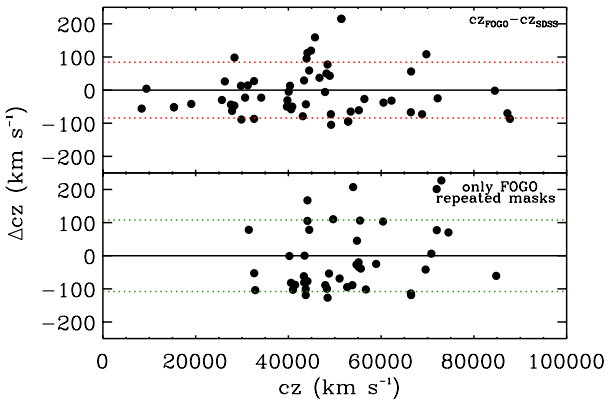

Fig. 3. Differences in LOS velocity for galaxies with both FOGO and SDSS measurements (*top panel*) and for galaxies with repeated FOGO measurements (*bottom panel*). Dotted lines represent the 1σ scatter of the data.

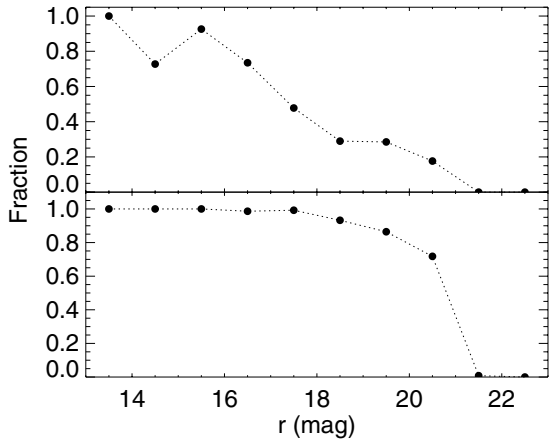

Fig. 4. Spectroscopic completeness of the 25 FG candidates with either FOGO or SDSS spectroscopy (*top panel*) and success rate of the 18 FG candidates with FOGO spectroscopy only (*bottom panel*) as a function of *r*-band magnitude.

is 84 km s^{-1}, which is consistent with the results of Sect. 4.1. Finally, for FGS05 we added the LOS velocities given by Girardi et al. (2006) and obtained with the same instrumental setup and data analysis.

4.3. Spectroscopic completeness

The completeness of the spectroscopic sample is a crucial parameter since it is used in the derivation of several quantities, such as the spectroscopic luminosity function. For each magnitude bin, we defined our completeness as the ratio between the number of galaxies of the 25 FG candidates for which we were able to obtain a redshift (N_z) from either the FOGO or SDSS spectroscopy and the number of targets ($N_{z_{\rm phot}}$, see Sect. 3.2):

$$C = \frac{N_z}{N_{z_{\rm phot}}}. \quad (1)$$

In Fig. 4 we show our completeness as a function of the *r*-band magnitude. Our sample is more than 70% complete down to $m_r = 17$ and more than 50% complete at $m_r = 18$.

In a similar way, for each magnitude bin, we defined the success rate as the ratio between the number of galaxies of the

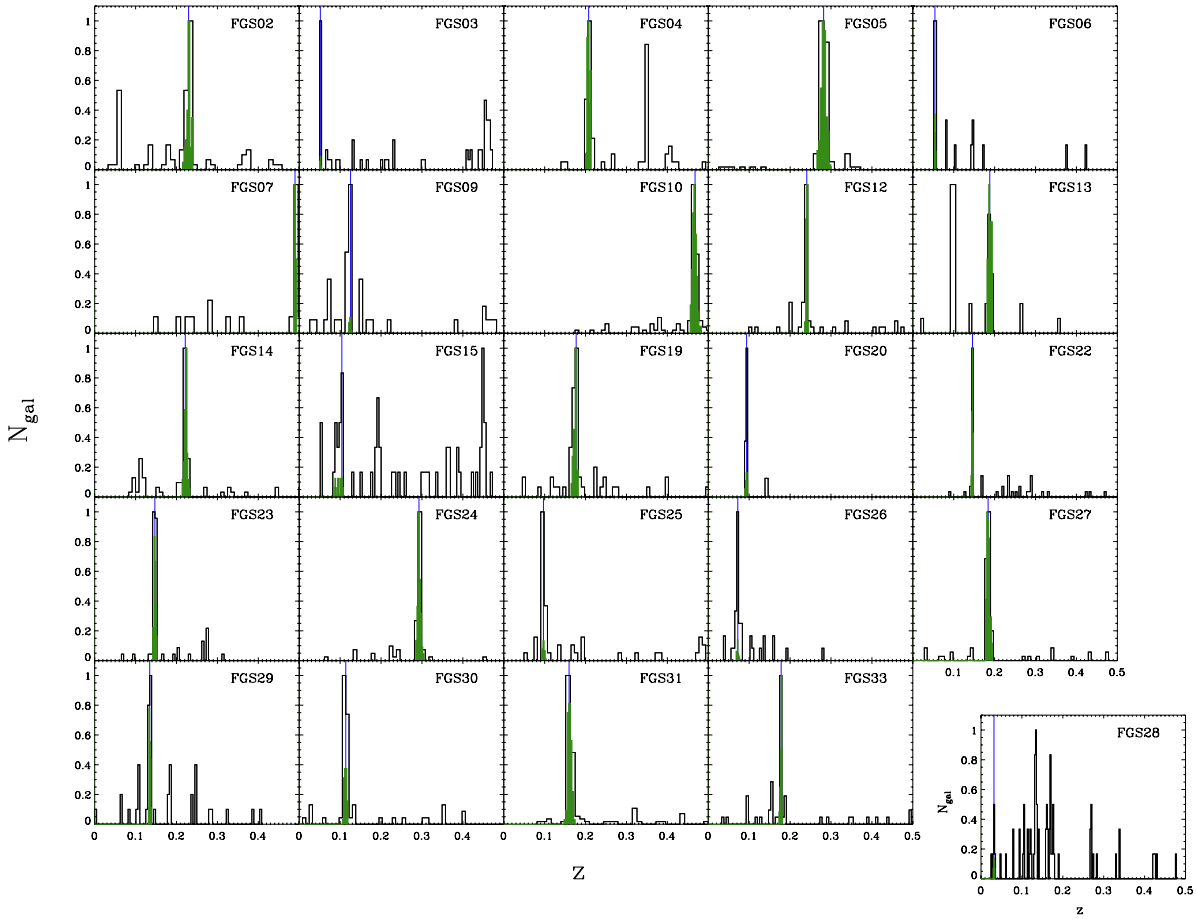

Fig. 5. Identification of the members of the 25 FG candidates in the redshift space. For each system we show all the galaxies in the field of view (black histogram), as well as the galaxies identified as members using the DEDICA procedure (green histogram) associated to the BGG (blue line). The peculiar case of FGS28 is shown separately.

18 FG candidates for which we are able to measure a redshift with our own spectroscopy ($N_{z_{\rm our}}$) and the total number of observed galaxies ($N_{\rm obs}$):

$$SR = \frac{N_{z_{\rm our}}}{N_{\rm obs}}. \quad (2)$$

Figure 4 also shows the success rate as a function of the r-band magnitude. We have a success rate over 75% for objects with $m_r < 21$. The success rate decreases abruptly at $m_r > 21$. Thus, we conclude that the adopted combination of instrumental setup and exposure time is effective for measuring the redshift of galaxies with $m_r \leq 21$.

5. Results

5.1. System membership

Both the identification of systems and the membership of individual galaxies were obtained using a two-step procedure applied to the galaxies in the region within R_{200}. First, we used DEDICA (Pisani 1996, 1993), which is an adaptive kernel procedure that works under the assumption that a cluster corresponds to a local maximum in the density of galaxies. Then, we adopted the likelihood ratio test (Materne 1979) to assign a membership probability to each single galaxy relative to an identified cluster.

According to the DEDICA procedure, each FG candidate was detected as a very significant peak (at a confidence level >99%) at the redshift corresponding to that of the BGG. Only FGS14, FGS23, and FGS26 were detected as two close peaks (with $\Delta v < 1500$ km s^{-1} in the rest frame). For each FG candidate, the redshift of the BGG, the redshift distribution of the galaxies, and the redshift peak associated to the BGG are shown in Fig. 5. Some structures are isolated (e.g., FGS20), while others present clear foreground (e.g., FGS07) or background (e.g., FGS15) contamination. The corresponding members were then identified using the distance–velocity diagram (Fig. 6), which consists in the so-called "shifting gapper" method (Fadda et al. 1996; Girardi et al. 1996). This procedure rejects galaxies within a fixed distance bin that are too far in velocity from the main body of the system. The distance bin is shifted outward to R_{200}. The procedure was then iterated until the number of cluster members converged to a stable value. Following Fadda et al. (1996), we used a velocity gap of 1000 km s^{-1} in the cluster rest frame and a distance bin of 0.6 Mpc (or large enough to include 10 galaxies). In the case of FGS02 we slightly modified the gap value (1100 km s^{-1}) to be more conservative and to avoid the rejection of a few galaxies at the edge of the system. For all the systems, our own spectroscopic data extend to at least 0.5 R_{200}, except for FGS28, FGS30, and FGS31 for which we covered 0.4 R_{200}. The membership efficiency, defined as the fraction of confirmed members with respect to the observed targets, turns out to be 59%.

FGS15 seems to be a peculiar case within the subsample of 25 FG candidates. It has only 13 members spanning a wide range in velocity between one another (up to 6000 km s^{-1}). Thus, it is not clear if either this system is very massive or it is part of a

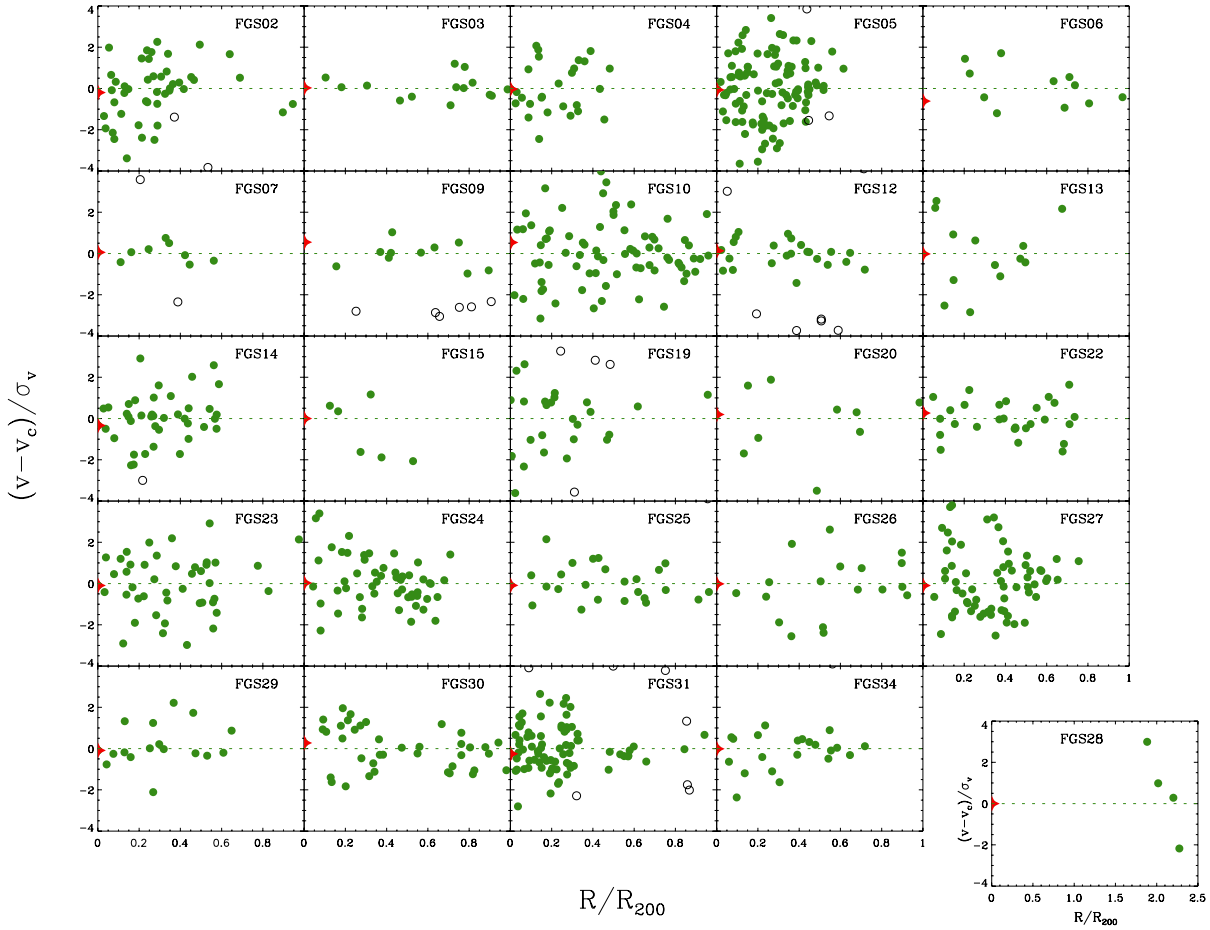

Fig. 6. Velocity–position diagram of the sample of FG candidates. Green filled and black open circles mark the member and non-member galaxies, respectively. The red star indicates the BGG. The peculiar case of FGS28 is shown apart.

larger structure, such as a filament. Another system with peculiar properties is FGS28. It is the smallest group of the Santos et al. (2007) sample. It has the faintest BGG and the lowest X-ray luminosity, and it seems much more an isolated giant elliptical galaxy than a group of galaxies. The peak associated to the BGG in the velocity histogram (Fig. 5) is not significant, and we found only four (possible) members that are at a distance about $2\,R_{200}$ of the group. We argue that this BGG is actually a large and isolated galaxy that is embedded in a high density environment owing to the presence of another cluster in the same region. For both FGS28 and FGS15, we used the membership only for calculating the magnitude gaps, but not for estimating the LOS velocity dispersion and mass.

5.2. Cluster global properties

In Table 1 we present the general properties for each system of the Santos et al. (2007) sample. We estimated R_{200} from L_X, which is available for each of the 34 FG candidates from the RASS Catalogs. We decided to recalculate L_X because of the discrepancies between the values reported by Santos et al. (2007) and other measurements available in the literature for some well studied clusters of their sample (e.g., A267 and A697, see Böhringer et al. 2000, after the adequate cosmology and band conversions). For each FG candidate, we took the counts from the RASS Bright Source Catalog (RASS-BSC, Voges et al. 1999) into account or, alternatively, from the RASS Faint Source Catalog (RASS-FSC, Voges et al. 2000) in the broad band 0.1−2.4 keV. We used the total Galactic column density (N_H) as taken from the NASA's HEASARC N_H tool[4] and the redshift z as listed by Santos et al. (2007). We used an iterative procedure based on PIMMS[5] (Mukai 1993). Details of the procedure are available in Girardi et al. (2014).

With our new L_X estimates, we were able to calculate R_{500} using the relation proposed by Böhringer et al. (2007, see their Eq. (2) for details):

$$R_{500} = 0.753\,\mathrm{Mpc}\,h_{100}^{-0.544}\,E(z)^{-1}\,L_{X,44}^{0.228} \quad (3)$$

where $E(z) = h(z)/h_0$ and $L_{X,44}$ is the X-ray luminosity in units of $h_{70}^{-2}10^{44}$ erg s^{-1} in the 0.1−0.24 keV band. We calculated $R_{200} = 1.516 \times R_{500}$ as prescribed by Arnaud et al. (2005).

We computed the mean LOS velocity dispersion σ_v by using the bi-weight estimator of the ROSTAT package (Beers et al. 1990) for systems with more than ten members. For the remaining systems, we computed σ_v using the bi-weight estimator and shifting gapper. We applied both the cosmological correction and standard correction for velocity uncertainties (Danese et al. 1980). By assuming sphericity and dynamical

[4] http://heasarc.gsfc.nasa.gov/cgi-bin/Tools/w3nh/w3nh.pl
[5] ftp://legacy.gsfc.nasa.gov/software/tools/pimms4_3.tar.gz

Table 1. Global properties of our sample.

Name	RA (J2000) (hh:mm:ss)	Dec (J2000) (°:′:″)	z	Δm_{12} (mag)	Δm_{14} (mag)	R_{200} (Mpc)	$N_{\rm vel}$ (# Gal)	$N_{\rm memb}$ (# Gal)	σ_v (km s^{-1})	M_v ($M_\odot$)
(1)	(2)	(3)	(4)	(5)	(6)	(7)	(8)	(9)	(10)	(11)
FGS01	01:50:21.3	–10:05:30.5	0.365	>1.41 ± 0.23	>1.61 ± 0.19	1.71	–	–	–	–
FGS02*	01:52:42.0	+01:00:25.6	0.230	>2.12 ± 0.33	>2.28 ± 0.33	1.85	111(65)	42	1263	1.87E+15
FGS03*	07:52:44.2	+45:56:57.4	0.052	2.09 ± 0.06	2.55 ± 0.08	0.96	89 (0)	16	259	4.20E+13
FGS04	08:07:30.8	+34:00:41.6	0.208	>1.65 ± 0.27	>2.04 ± 0.25	1.44	65 (64)	28	852	6.67E+14
FGS05	08:42:57.6	+36:21:59.3	0.282	1.12 ± 0.07	>1.85 ± 0.07	2.11	134 (82)	108	1516	3.06E+15
FGS06	08:44:56.6	+42:58:35.7	0.054	0.20 ± 0.12	2.11 ± 0.17	0.72	21 (0)	12	330	5.18E+13
FGS07	09:03:03.2	+27:39:29.4	0, 489	1.32 ± 0.33	1.96 ± 0.35	1.68	28 (27)	11	926	8.94E+14
FGS08*	09:48:29.0	+49:55:06.7	0, 409	>2.12 ± 0.16	>2.17 ± 0.14	1.29	–	–	–	–
FGS09	10:43:02.6	+00:54:18.3	0, 125	0.40 ± 0.30	>0.68 ± 0.31	1.55	58 (0)	11	493	2.42E+14
FGS10**	10:54:52.0	+55:21:12.5	0, 468	2.12 ± 0.33	2.24 ± 0.29	1.43	116 (115)	78	969	8.32E+14
FGS11	11:14:39.8	+40:37:35.2	0, 202	>0.62 ± 0.11	>1.03 ± 0.06	1.34	47 (0)	0	–	–
FGS12	11:21:55.3	+10:49:23.2	0, 240	1.61 ± 0.19	>2.00 ± 0.20	1.34	54 (53)	24	378	1.22E+14
FGS13	11:41:28.3	+05:58:29.5	0, 188	1.23 ± 0.27	>1.80 ± 0.27	1.19	40 (39)	14	937	6.70E+14
FGS14*	11:46:47.6	+09:52:28.2	0, 221	1.96 ± 0.29	2.43 ± 0.35	1.45	78 (77)	40	774	5.55E+14
FGS15[a]	11:48:03.8	+56:54:25.6	0, 105	1.83 ± 0.09	2.27 ± 0.05	0.98	63 (50)	13	–	–
FGS16	11:49:15.0	+48:11:04.9	0, 283	>0.98 ± 0.33	>1.13 ± 0.32	1.45	–	–	–	–
FGS17*	12:47:42.1	+41:31:37.7	0, 155	1.96 ± 0.55	>2.7 ± 0.23	0.87	–	–	–	–
FGS18	13:00:09.4	+44:43:01.3	0, 233	>1.41 ± 0.27	>1.72 ± 0.29	1.17	–	–	–	–
FGS19	13:35:60.0	–03:31:29.2	0, 177	1.35 ± 0.23	1.97 ± 0.28	1.37	57 (43)	25	978	8.35E+14
FGS20*	14:10:04.2	+41:45:20.9	0, 094	2.17 ± 0.15	>2.46 ± 0.14	0.74	12 (0)	10	578	1.63E+14
FGS21	14:45:16.9	+00:39:34.3	0, 306	<0.00 ± 0.19	>0.84 ± 0.26	1.53	–	–	–	–
FGS22	14:53:59.0	+48:24:17.1	0, 146	1.49 ± 0.14	2.28 ± 0.14	0.87	60 (57)	29	323	5.92E+13
FGS23*	15:29:46.3	+44:08:04.2	0, 148	1.87 ± 0.18	>2.64 ± 0.14	1.02	63 (60)	45	659	2.86E+14
FGS24	15:33:44.1	+03:36:57.5	0, 293	0.33 ± 0.15	1.08 ± 0.20	1.49	73 (69)	55	780	5.75E+14
FGS25	15:39:50.8	+30:43:04.0	0, 097	1.12 ± 0.22	1.68 ± 0.29	1.50	70 (0)	25	645	4.04E+14
FGS26*	15:48:55.9	+08:50:44.4	0, 072	1.18 ± 0.20	>3.22 ± 0.19	0.90	38 (0)	20	675	2.67E+14
FGS27*	16:14:31.1	+26:43:50.4	0, 184	1.61 ± 0.22	2.64 ± 0.21	1.26	94 (88)	66	910	6.69E+14
FGS28*,[a]	16:37:20.5	+41:11:20.3	0, 032	>3.28 ± 0.07	>3.68 ± 0.08	0.47	76 (27)	1	–	–
FGS29*	16:47:02.1	+38:50:04.3	0, 135	1.81 ± 0.21	2.55 ± 0.22	0.89	46 (42)	18	408	9.66E+13
FGS30*	17:18:11.9	+56:39:56.1	0, 114	1.84 ± 0.14	2.08 ± 0.14	1.47	63 (28)	39	765	5.57E+14
FGS31	17:20:10.0	+26:37:32.1	0, 159	>1.04 ± 0.25	>1.40 ± 0.23	2.02	132 (89)	80	1064	1.46E+15
FGS32*	17:28:52.2	+55:16:40.8	0, 148	>1.28 ± 0.26	>2.48 ± 0.16	0.78	–	–	–	–
FGS33	22:56:30.0	–00:32:10.8	0, 224	>1.11 ± 0.14	>1.15 ± 0.13	1.24	–	–	–	–
FGS34*	23:58:15.1	+15:05:43.6	0, 178	1.82 ± 0.28	>3.09 ± 0.36	1.00	52 (47)	22	360	8.36E+13

Notes. Column (1): system number as in Santos et al. (2007); Col. (2): right ascension of the BGG; Col. (3): declination of the BGG; Col. (4): redshift of the BGG; Col. (5): gap in magnitude between the two brightest member galaxies; Col. (6): gap in magnitude between the brightest and the fourth brightest member galaxies; Col. (7): estimation of the virial radius of the system derived from L_X; Col. (8): number of velocities available within R_{200}. The number of new velocities from our own observations is given in parenthesis; Col. (9): number of spectroscopically confirmed members; Col. (10): velocity dispersion of the system; Col. (11): mass of the system within 0.5 R_{200}, from Eq. (4). [(*)] Fossil system according to our definition. [(**)] For homogeneity, we recomputed the gaps for this system that we analyzed in Aguerri et al. (2011). In particular, we used 0.5 R_{200} and only three different magnitudes to calculate Δm_{12} and Δm_{14}. [(a)] System with not reliable membership determination for which we did not compute σ_v and M_v.

equilibrium and also that galaxy distribution traces mass distribution, we followed Girardi et al. (1998) and Girardi & Mezzetti (2001) to compute the virial mass as

$$M_{\rm v} = \frac{3\pi}{2G}\sigma_v R_{\rm pv} - {\rm SPT}, \quad (4)$$

where SPT is the surface pressure term correction (The & White 1986), while $R_{\rm pv}$ is two times the projected mean harmonic radius. We could not compute $R_{\rm pv}$ by using data of observed galaxies since our z data do not cover the whole R_{200} region. Therefore, we used an alternative estimate that is valid for a typical galaxy distribution in clusters (see Eq. (13) of Girardi et al. 1998). We assumed 20% for the SPT correction, as obtained by combining data on many clusters and valid at a radius around R_{200} (Carlberg et al. 1997; Girardi et al. 1998).

5.3. $L_{\rm X}$–σ_v relation

Once we obtained the luminosity in X-ray and velocity dispersion of the galaxies, we were able to evaluate the $L_{\rm X}$–σ_v relation. This relation is connected with the formation of the cluster. In fact, theoretical predictions based on purely gravitational collapse lead to $L_{\rm X} \propto \sigma_v^4$. There are several observational studies of this relation, the majority of them finding values between 4 and 5.3 for the slope (Quintana & Melnick 1982; Edge & Stewart 1991; Mulchaey & Zabludoff 1998; Borgani et al. 1999; Xue & Wu 2000; Mahdavi & Geller 2001; Girardi & Mezzetti 2001; Ortiz-Gil et al. 2004; Hilton et al. 2005). In Fig. 7 we show the distribution and best fit to our data. We found a slope consistent within the errors to the theoretical predictions. We derived the best-fit $L_{\rm X}$–σ_v relation using the FITEXY algorithm

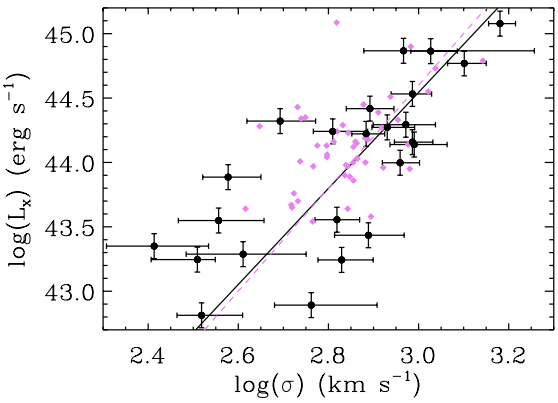

Fig. 7. L_X–σ_v relation for the FG candidates for which we were able to determine a velocity dispersion. The black circles represent our data and violet diamonds are taken from Cava et al. (2009) for comparison. The solid black line is our best fit and the dashed violet line is the best fit from Cava et al. (2009).

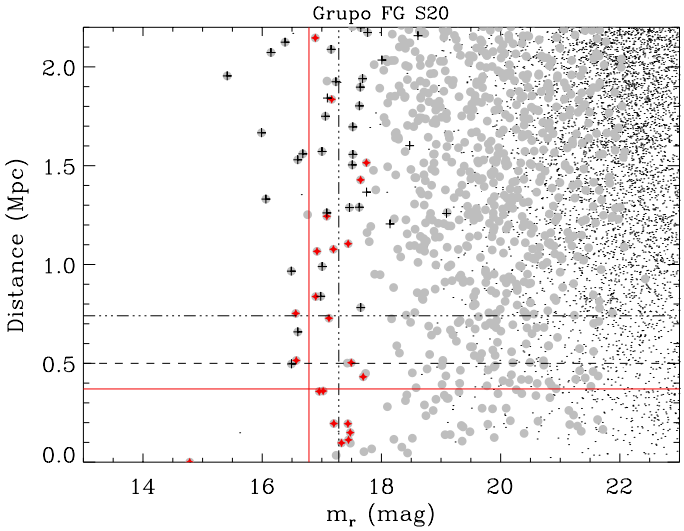

Fig. 8. Magnitude–distance diagram for the group FGS20. The distance from the BGG is given as a function of the magnitude for each galaxy. The black points represent all the galaxies within the FoV, gray circles are the target galaxies (see Sect. 3.2 for details), red stars represent the spectroscopically confirmed members, and black crosses are the spectroscopically confirmed non-members. The horizontal solid red line corresponds to 0.5 R_{200}, the dash-dotted black line marks R_{200}, and the dashed black line represents 0.5 Mpc, which is the limit used by Santos et al. (2007) to define the fossilness of the group. The solid red and dash-dotted vertical lines indicate the 2-mag and 2.5-mag gaps from the BGG, which determine the fossilness of the group following the criteria by Jones et al. (2003) and Dariush et al. (2010), respectively.

in IDL[6] which account for measurements uncertainties in both variables.The ROSTAT package gave us the uncertainties in the velocity dispersion measurements, while for the X-ray luminosity we used the counts uncertainties listed by RASS-BCS/FSC and computed the relative error. The same relative error was assumed for L_X, and we found a median value of $\sigma_{L_X} \sim 25\%$. Our best-fitting relation is

$$\log(L_X) = (33.35 \pm 0.73) + (3.72 \pm 0.26)\log(\sigma_v). \quad (5)$$

This relation is shown in Fig. 7 together with the L_X–σ_v relation for the WINGS nearby cluster sample (Fasano et al. 2006; Cava et al. 2009). The two relations are in good agreement with one another.

5.4. Fossilness determination

A fossil system is defined as having a large gap in magnitude in the *r*-band between the two brightest members of the system, namely larger than two magnitues within 0.5 R_{200}. We calculated the distance from the BGG and magnitude for each galaxy to verify the fossilness criterium of our sample. In this way, we obtained a diagram (such as that shown in Fig. 8) that allowed us to constrain the main properties of the system, such as the magnitude gap, virial radius, cluster membership, and magnitude of the BGG.

The magnitudes of the galaxies were obtained from SDSS-DR7 and our own photometry (see Sect. 3.1). We used the extinction-corrected Petrosian and model *r*-band magnitudes for all the objects in the SDSS-DR7 database. In addition, we have our own photometry for 30 out of 34 galaxy systems. Our photometry only covers the central regions of the clusters but it is about two magnitudes deeper in the *r*-band (see Fig. 8). We ran SExtractor (Bertin & Arnouts 1996) on our images to obtain the *r*-band MAG-BEST[7] magnitude.

Determining the magnitude of the BGGs is not straightforward. In SExtractor a successful deblending strongly depends on both the angular size of the BGG and the number of its close satellites. To circumvent this problem, we recomputed the magnitude of the BGGs using an ad hoc procedure on our images. In particular, we modeled the light of the BGGs by masking its close satellites. The model was done in IRAF by using the `bmodel` task, which adopts the isophotal fit of the galaxy provided by `ellipse` as input (Jedrzejewski 1987). The magnitude of the BGGs was computed using these uncontaminated models. Besides this, the modeled light of the BGGs was subtracted from the original images, and the magnitudes of all other galaxies were obtained by running SExtractor in the resulting images. SDSS photometry suffers from both deblending and overestimation of sky levels near bright galaxies (Blanton et al. 2011).

The final magnitude of each galaxy was obtained by averaging the available magnitudes to have a more realistic estimate of the uncertainty. This was computed as the rms of the available magnitudes. Table 1 presents the value of the gap between the two brightest (Δm_{12}) and the first and fourth ranked galaxies (Δm_{14}) within 0.5 R_{200} for each system. Some gaps are marked as lower limits because our spectroscopy failed to determine a redshift for some "bright" target galaxy (see Sect. 4.3 for details). For this reason we were not able to assign membership to these objects.

According to Jones et al. (2003) and Dariush et al. (2010), a system is a fossil if $\Delta m_{12} \geq 2.0$ or $\Delta m_{14} \geq 2.5$ mag, respectively. We considered as fossil systems those that satisfy at least one of the previous criteria taking the errors in the magnitude gaps determination into account. More explicitly, a system is a fossil if $\Delta m_{12} + \epsilon_{12} \geq 2.0$ or $\Delta m_{14} + \epsilon_{14} \geq 2.5$, where ϵ_{12} and ϵ_{14} are the 1σ uncertainties in the magnitude gaps. In Table 1 we highlighted the 15 systems that follow the previous criteria. The two methods find 12 and 13 fossil systems, even though

[6] Interactive Data Language is distributed by ITT Visual Information Solution. It is available from `http://www.ittvis.com/`

[7] MAG-BEST is an aperture magnitude, that enclosed the total light of the galaxy. It usually coincides with MAG-AUTO, which is the best total magnitude provided for galaxies by SExtractor. The latter provides MAG-ISOCOR instead of MAG-AUTO if the galaxy is at least 10% contaminated by another object.

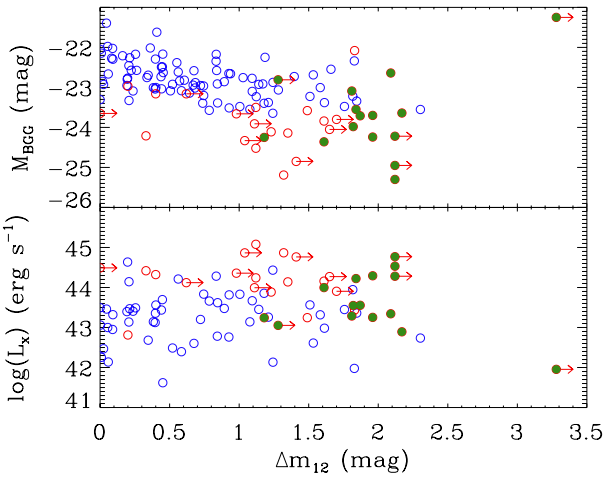

Fig. 9. Absolute r-band magnitude of the BGG (*top panel*) and X-ray luminosity of the system (*bottom panel*) as a function of the gap in magnitude between the two brightest galaxies of the systems studied in this paper (open red circles) and in Aguerri et al. (2007, open blue circles). The green filled circles are the genuine fossil systems. The points with a right arrow are those systems for which the magnitude gap is a lower limit.

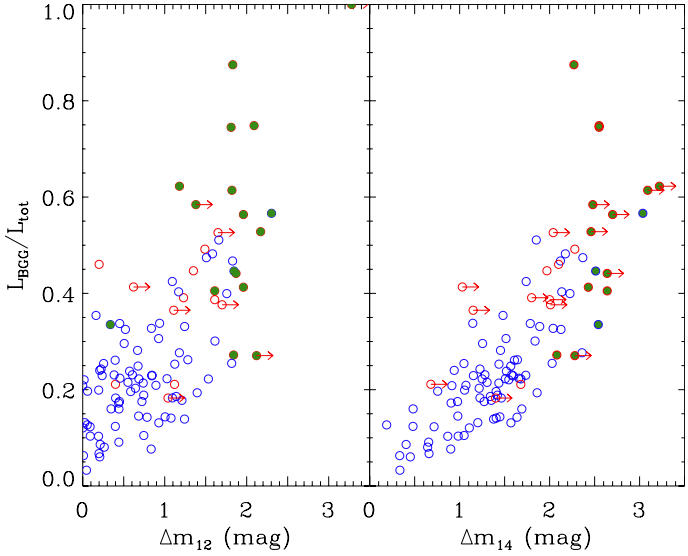

Fig. 10. Fraction of light of the BGG as function of Δm_{12} and Δm_{14} for the systems studied in this paper (open red circles) and in Aguerri et al. (2007, open blue circles) with $z \leq 0.25$. The filled green circles represent the genuine fossil systems. The points with a right arrow are those systems for which the magnitude gap is a lower limit.

Dariush et al. (2010) claim that their method is expected to find 50% more fossil systems than Jones et al. (2003).

The fossil definitions take not only the magnitude gaps but also the virial radius of the system into account. Thus, uncertainties in the R_{200} determination reflect in uncertainties in the fossil classification. Therefore, we computed the variation in the number of fossil systems considering a 25% uncertainty in R_{200} in agreement with Girardi et al. (2014). The number of fossil systems is 15^{+8}_{-4}. The upper limit gives the number of fossil systems for a 25% smaller R_{200}. Similarly, the lower limit corresponds to the number of fossil systems for a 25% larger R_{200}.

5.5. Correlations with the magnitude gaps

In Fig. 9 we show Δm_{12} as a function of both the absolute r-band magnitude of the BGG ($M_{\rm BGG}$) and X-ray luminosity of the system. Our FG candidates mainly show $\Delta m_{12} > 1$. To have more clusters in the range $0 < \Delta m_{12} < 1$, we included the sample of nearby ($z < 0.1$) galaxy clusters from Aguerri et al. (2007). Their Δm_{12} was obtained from spectroscopically confirmed members within 0.5 R_{200} once we applied the same evolutionary and K corrections that we used for the Santos et al. (2007) sample. For both relations we computed the Spearman correlation coefficients. We found a strong correlation (significance $>3\sigma$) between Δm_{12} and $M_{\rm BGG}$. On average, the larger Δm_{12}, the brighter the central objects. The $M_{\rm BGG}$ and Δm_{12} correlation is somewhat expected in the classical scenario of the formation of fossil systems, in which the central galaxy has grown by merging with nearby L^* galaxies. A similar correlation was also observed for central galaxies in other cluster samples (see Ascaso et al. 2011, and references therein). In contrast, the relationship between $\log(L_{\rm X})$ and Δm_{12} is weaker (significance $<2\sigma$).

We also analyzed the fraction of total optical luminosity contained within the central galaxy ($L_{\rm BGG}/L_{\rm tot}$) as a function of the magnitude gaps Δm_{12} and Δm_{14}. In this case, the total luminosity $L_{\rm tot}$ represents the sum of the luminosities of all the galaxies with $|(g-r)-(g-r)_{BGG}| \leq 0.2$, $M_{\rm r} \leq -20.0$, and within 0.5 R_{200}. We limited this analysis to systems with $z \leq 0.25$ because we were unable to reach $M_{\rm r} = -20.0$ for more distant systems. Figure 10 shows a clear correlation (Spearman test significance $>3\sigma$) between $L_{\rm BGG}/L_{\rm tot}$ and the two magnitude gaps. Fossil systems are, on average, those objects with a larger fraction of light in the BGG. Nevertheless, they are characterized by a wide range of $L_{\rm BGG}/L_{\rm tot}$ values ($0.25 < L_{\rm BGG}/L_{\rm tot} < 0.75$). Most of the systems with $L_{\rm BGG}/L_{\rm tot} > 0.5$ are fossil ones. Similar relations were also found in other fossil samples (see Harrison et al. 2012), and recently Shen et al. (2014) have suggested that the growth in mass of the BGGs is directly correlated with Δm_{12} and that this correlation is needed to justify the BGGs over luminosity.

Fossil systems always represent extreme cases in the correlations. However, Figs. 9 and 10 indicate that not all the properties of the clusters depend on Δm_{12}.

5.6. Correlation with the velocity dispersion

In Fig. 11 we show the correlation between the fraction of light enclosed in the BGG ($L_{\rm BGG}/L_{\rm tot}$) as a function of the LOS velocity dispersion σ_v of the cluster for the same sample of Fig. 9. This is a well known correlation that was originally reported by Lin & Mohr (2004). They argue that this correlation, together with the correlation between the luminosity of the BGGs and the mass of the system, indicates that BGGs grow by merging galaxies. In addition, they claim that the decrease in the BGG luminosity fraction with cluster mass indicates that the rate of luminosity growth of the BGGs is slower than the rate at which clusters acquire galaxies from the field.

Figure 11 clearly shows that fossil systems delineate the upper envelope of the expected trend of the $L_{\rm BGG}/L_{\rm tot}$–σ_v relation of non-fossil systems, so for a given velocity dispersion (or mass), fossil systems have a larger fraction of light enclosed in the BGG. Following Lin & Mohr, we infer that the growth rate of BGGs in fossil systems is greater than that of BGGs in non-fossil systems. Non-fossil systems that are located in the upper envelope of Fig. 11 have either large gaps in magnitude or gaps calculated only as lower limits. The former are systems dominated by the BGG, which are classified as non-fossil systems

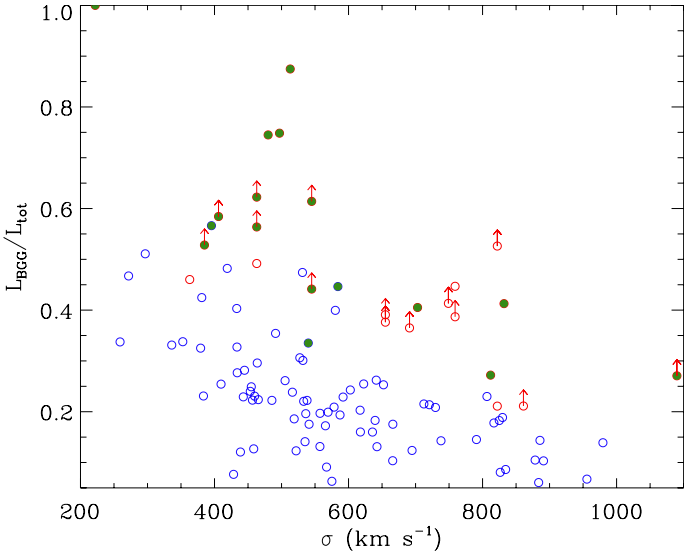

Fig. 11. Fraction of light of the BGG as function of the LOS velocity dispersion (mass) of the system. The symbols and colors are the same as in Fig. 10. Upward arrows indicate those systems for which the magnitude gaps (and thus the L_{BGG}/L_{tot}) represent lower limits.

only due to the arbitrariness of the fossilness criteria. The latter are expected to be genuine fossil systems, but for which further investigation is needed to constrain Δm_{12} and Δm_{14}.

6. Discussion

6.1. Differences with Santos et al. (2007)

We carefully analyzed the sample of FG candidates presented by Santos et al. (2007). As they claim, the number of fossil systems depends critically on the parameters adopted for measuring the magnitude gaps. It is thus very important to highlight the differences between theirs and our methodologies. First of all, Santos et al. (2007) used a fixed radius to look for the second brightest galaxies, namely 0.5 Mpc, whereas we were able to compute the virial radius for each cluster from its X-ray luminosity. The value of 0.5 R_{200} that we obtained for the Santos et al. (2007) candidates varies between 0.29 Mpc and 1.02 Mpc, with a mean value of 0.63 Mpc. This means that, on average, the radius within which we looked for the second brightest galaxies is larger than the one adopted in Santos et al. (2007). Therefore, we expect that not all the candidates proposed by Santos et al. (2007) are genuine fossil systems.

Moreover, the procedure for defining cluster membership adopted by Santos et al. (2007) suffers from three main problems. First, only a few spectroscopic redshifts were available in the SDSS-DR5 for the 34 FG candidates. Second, Santos et al. (2007) considered all the galaxies with the spectroscopic redshift in the range $z_c \pm \Delta z$ as members, where z_c is the cluster redshift and $\Delta z = 0.002$. It is worth noting that Δz was fixed for all the clusters, and did not take the differences in velocity dispersion (or mass) between the systems into account. Third, Santos et al. (2007) also considered as cluster members the galaxies without the spectroscopic redshift but with a photometric redshift in the range $z_c \pm 0.035$. This photometric redshift window is too small to deal with the typical errors of 0.1 expected for SDSS-DR5 photometric redshifts. In addition, they only considered galaxies with errors smaller than 0.1 in the photometric redshift.

In contrast, we were able to obtain a number of spectroscopic velocities good enough to compute the LOS velocity dispersion of the systems and to accurately define the cluster membership. In particular, for 25 out of 34 systems, the cluster membership was obtained using a two-step method of member selection that works both in the redshift space and projected space phase. This method is much more robust than the simple z-cut proposed by Santos et al. (2007). Moreover, our photometric redshift criterion for membership adopts a much larger window of $z_c \pm 0.15$. For all these reasons, it is not surprising that only half of the systems proposed by Santos et al. (2007) as FG candidates turned out to be genuine fossil systems according to our criteria. Finally, it is important to notice that there are 12 systems in the sample that are not fossils but the magnitude gaps we calculated for them are only lower limits. This means that, in principle, there could be other genuine fossil systems in the sample, which could be identified by completing the spectroscopic survey.

6.2. Formation scenarios for fossil systems

There are two models that are mainly used in the literature to explain the formation scenarios for fossil systems. The first and widely accepted one (D'Onghia et al. 2005; Sommer-Larsen 2006; von Benda-Beckmann et al. 2008; Dariush et al. 2010, among others) is that fossil systems were assembled at a higher redshift than regular clusters and, due to particularly favorable conditions, they had enough time to merge L^* galaxies in a single giant BGG. This process results in the observed gap in magnitude that is a consequence of the system evolution. The second scenario (Mulchaey & Zabludoff 1999) suggests that the BGG was created in a single monolithic collapse and that the gap in magnitude is present from the beginning. The two formation processes are called the *merging* and the *failed group* scenario, respectively.

The observational properties of our systems are the following:

(a) Fossil systems are observed at any LOS velocity dispersion (mass) of the host DM halo (Table 1). Indeed, we have both fossil groups and fossil clusters.
(b) Systems with larger Δm_{12} have brighter BGGs (Fig. 9, top panel).
(c) Systems with larger Δm_{12} or Δm_{14} have a greater fraction of total galaxy light contained within the BGG (Fig. 10).
(d) Fossil systems follow the same L_{BGG}/L_{tot}–σ_v relation of non-fossil systems. However, fossil systems are extreme cases of this relation and show higher L_{BGG}/L_{tot} for a fixed LOS velocity dispersion (Fig. 11).
(e) Fossil systems verify the same L_X–σ_v relation as non-fossil systems.

All these facts can be interpreted in the terms of the merging scenario: the fossil systems are the result of massive merger episodes in the early Universe because their galaxies follow more low angular momentum orbits than galaxies in non-fossil systems. In this case, the observed magnitude gap is an indication of the evolutionary state of the system. Thus, the systems with larger magnitude gaps are expected to have brighter central galaxies and a greater fraction of light enclosed in their BGGs. The growth of the BGG in fossil systems is stronger than in non-fossil ones, but it is expected to follow the same rules of normal clusters (see Lin & Mohr 2004).

The properties we observed in fossil systems can also be explained by the failed group scenario. Nevertheless, there are other properties that seem to disfavor this scenario. For example, the monolithic formation of elliptical galaxies predicts strong metallicity gradients, whereas the stellar population gradients

are erased by mergers. In this context, Eigenthaler & Zeilinger (2013) find flat age and metallicity gradients for a sample of central galaxies in fossil systems,which are not compatible with the failed group scenario. Moreover, the bend observed at high masses in the scaling relations of early-type galaxies also suggests that fossil systems were formed by mergers (see Bernardi et al. 2011). In particular, for the BGGs of our 34 FG candidates, a two-phase merger scenario was proposed to explain their scaling relations. Indeed, Méndez-Abreu et al. (2012) claim that these objects went through dissipational mergers in an early stage of their evolution and assembled the bulk of their mass through subsequent dry mergers. This process seems similar to the one proposed by Díaz-Giménez et al. (2008), in which the BGGs in fossil systems have undergone their last major merger later than in non-fossil systems.

6.3. Transitional fossil systems

The correlation between the gap in magnitude and absolute magnitude of the BGG suggests that the scenario that suggests the existence of transitional fossil systems (von Benda-Beckmann et al. 2008) cannot be applied to those systems with the brightest BGGs. In fact, the probability that two systems with such a bright central galaxy would merge is negligible. For this reason, we expect that current fossil systems hosting the most luminous BGGs will be fossils forever. Nevertheless, the von Benda-Beckmann et al. (2008) scenario could explain the case of FGS06. The BGG has a magnitude of $M_r = -22.88$, whereas the second ranked one, located at $\sim 0.4\ R_{200}$, has $M_r = -22.68$. These magnitude values are typical of central galaxies in groups and clusters (see Fig. 9). The third, fourth, and fifth ranked galaxies have magnitudes of $M_r = -21.19$, -20.77, and -20.18, respectively. Moreover, FGS06 is the only non-fossil system in our sample with an abrupt change in its magnitude gap if the second ranked galaxy was not considered. In fact, the median value of the magnitude gap change for non-fossil systems in our sample is 0.2 ± 0.2 mag, whereas FGS06 would suffer a 1.6 mag change. For these reasons, we suggest that FGS06 could be a good candidate for a transitional fossil systems such as those described by von Benda-Beckmann et al. (2008).

7. Conclusions

We characterized the sample of 34 FG candidates proposed by Santos et al. (2007) by using a unique collection of new optical photometric and spectroscopic data. This dataset was completed with SDSS-DR7 archival data. This large collection of radial velocities provided robust cluster membership and global cluster properties for a subsample of 25 systems that have not been available before.

The fossilness determination of the 34 FG candidates was revisited. In particular, the magnitudes of the galaxies in each system were obtained by averaging three different magnitudes: Petrosian and model magnitudes from SDSS-DR7 and MAG-BEST SExtractor magnitude from our data. This was done because the magnitude of the BGGs can be affected by close satellites both in the SDSS and SExtractor analyses. Therefore, we computed new magnitude gaps (Δm_{12} and Δm_{14}) within $0.5\ R_{200}$ for each system. The systems with $\Delta m_{12} \geq 2$ or $\Delta m_{14} \geq 2.5$ mag within the errors were classified as fossils. By applying this criterion, the total number of fossil systems in the sample is 15^{+8}_{-4}. The uncertainties in the total number of fossil systems reflect the uncertainties in the R_{200} determination. Moreover, there are 12 systems for which one or both the magnitude gaps are lower limits. For these systems, a more extended spectroscopic survey is needed in order to define their fossilness.

We derived the main observational properties of the fossil systems in our sample. The fossil systems span a wide range of masses, and we can confirm the existence of genuine fossil clusters in our sample. In particular, five fossil systems have LOS velocity dispersions $\sigma_v > 700\ \mathrm{km\,s^{-1}}$, from both the L_X luminosity and "shifting gapper" procedure. Clear correlations were found between the magnitude gaps and luminosity of the BGGs. In particular, the systems with larger Δm_{12} have brighter BGGs, and the systems with larger Δm_{12} or Δm_{14} have a larger fraction of the total galaxy light in the BGGs. The fossil systems also follow the same $L_{\mathrm{BGG}}/L_{\mathrm{tot}}$–$\sigma_v$ relation of non-fossil systems. Nevertheless, they are extreme cases in the studied relations. In particular, the fossil systems have brighter BGGs than normal systems for any given LOS velocity dispersion (mass).

All these properties can be explained by the two mainly accepted proposed scenarios for the formation of fossil structures so are not conclusive in this sense. Nevertheless, we suggest that fossil systems with very bright central galaxies are not transitional phases of regular clusters and groups because, if this was the case, we should find systems with small gaps but very bright and massive central galaxies. These systems are not observed because the probability that two systems with such a bright BGG would merge is negligible. On the contrary, the systems with fainter BGGs possibly experienced a transitional fossil stage, which ended by merging with another galaxy system. This could be the case of FGS06.

The FOGO project will continue in the near future by analyzing other observational properties of fossil systems. In a forthcoming paper, we will focus on the LFs of fossil and normal systems. This analysis will be crucial for understanding the formation and evolution of these galaxy aggregations, because the LFs of fossil systems in the merging scenario are expected to lack L^* galaxies. In contrast, the failed group formation scenario expects to find differences between fossil and normal systems in both the bright and faint ends of the LFs.

Acknowledgements. We would like to thank the anonymous referee for useful comments that helped us improve the paper. This work was partially funded by the Spanish MICINN (grant AYA2010-21887-C04-04), and the local Canarian Government (grant ProID20100140). This article is based on observations made with the *Isaac Newton* Telescope, Nordic Optical Telescope, and Telescope Nazionale *Galileo* operated on the island of La Palma by the Isaac Newton Group, the Nordic Optical Telescope Scientific Association, and the Fundación Galileo Galilei of the INAF (Istituto Nazionale di Astrofisica), respectively, in the Spanish Observatorio del Roque de los Muchachos of the Instituto de Astrofísica de Canarias. E.D. gratefully acknowledges support from the Alfred P. Sloan Foundation. M.G. acknowledges financial support from the MIUR PRIN/2010−2011 (J91J12000450001). E.M.C. is supported by Padua University (grants 60A02-1283/10,5052/11, 4807/12). J.I.P. and J.V.M. acknowledge financial support from the Spanish MINECO under grant AYA2010-21887-C04-01, and from Junta de Andalucía Excellence Project PEX2011-FQM7058. J.M.A. acknowledges support from the European Research Council Starting Grant (SEDmorph; P.I. V. Wild).

References

Adelman-McCarthy, J. K., Agüeros, M. A., Allam, S. S., et al. 2007, ApJS, 172, 634
Adelman-McCarthy, J. K., Agüeros, M. A., Allam, S. S., et al. 2008, ApJS, 175, 297
Aguerri, J. A. L., Sánchez-Janssen, R., & Muñoz-Tuñón, C. 2007, A&A, 471, 17
Aguerri, J. A. L., Girardi, M., Boschin, W., et al. 2011, A&A, 527, A143
Arnaud, M., Pointecouteau, E., & Pratt, G. W. 2005, A&A, 441, 893
Ascaso, B., Aguerri, J. A. L., Varela, J., et al. 2011, ApJ, 726, 69

Bardelli, S., Zucca, E., Vettolani, G., et al. 1994, MNRAS, 267, 665
Barrena, R., Girardi, M., Boschin, W., & Dasí, M. 2009, A&A, 503, 357
Beers, T. C., Flynn, K., & Gebhardt, K. 1990, AJ, 100, 32
Bernardi, M., Roche, N., Shankar, F., & Sheth, R. K. 2011, MNRAS, 412, 684
Bertin, E., & Arnouts, S. 1996, A&AS, 117, 393
Blanton, M. R., Kazin, E., Muna, D., Weaver, B. A., & Price-Whelan, A. 2011, AJ, 142, 31
Böhringer, H., Voges, W., Huchra, J. P., et al. 2000, ApJS, 129, 435
Böhringer, H., Schuecker, P., Pratt, G. W., et al. 2007, A&A, 469, 363
Borgani, S., Girardi, M., Carlberg, R. G., Yee, H. K. C., & Ellingson, E. 1999, ApJ, 527, 561
Boylan-Kolchin, M., Ma, C.-P., & Quataert, E. 2008, MNRAS, 383, 93
Carlberg, R. G., Yee, H. K. C., & Ellingson, E. 1997, ApJ, 478, 462
Cava, A., Bettoni, D., Poggianti, B. M., et al. 2009, A&A, 495, 707
Cypriano, E. S., Mendes de Oliveira, C. L., & Sodré, L., Jr. 2006, AJ, 132, 514
D'Onghia, E., Sommer-Larsen, J., Romeo, A. D., et al. 2005, ApJ, 630, L109
Danese, L., de Zotti, G., & di Tullio, G. 1980, A&A, 82, 322
Dariush, A., Khosroshahi, H. G., Ponman, T. J., et al. 2007, MNRAS, 382, 433
Dariush, A. A., Raychaudhury, S., Ponman, T. J., et al. 2010, MNRAS, 405, 1873
Díaz-Giménez, E., Muriel, H., & Mendes de Oliveira, C. 2008, A&A, 490, 965
Démoclès, J., Pratt, G. W., Pierini, D., et al. 2010, A&A, 517, A52
Edge, A. C., & Stewart, G. C. 1991, MNRAS, 252, 414
Eigenthaler, P., & Zeilinger, W. W. 2013, A&A, 553, A99
Eisenstein, D. J., Annis, J., Gunn, J. E., et al. 2001, AJ, 122, 2267
Ellingson, E., & Yee, H. K. C. 1994, ApJS, 92, 33
Fadda, D., Girardi, M., Giuricin, G., Mardirossian, F., & Mezzetti, M. 1996, ApJ, 473, 670
Fasano, G., Marmo, C., Varela, J., et al. 2006, A&A, 445, 805
Girardi, M., & Mezzetti, M. 2001, ApJ, 548, 79
Girardi, M., Fadda, D., Giuricin, G., et al. 1996, ApJ, 457, 61
Girardi, M., Giuricin, G., Mardirossian, F., Mezzetti, M., & Boschin, W. 1998, ApJ, 505, 74
Girardi, M., Boschin, W., & Barrena, R. 2006, A&A, 455, 45
Girardi, M., Aguerri, J. A. L., De Grandis, S., et al. 2014, A&A, 565, A115
Harrison, C. D., Miller, C. J., Richards, J. W., et al. 2012, ApJ, 752, 12
Hilton, M., Collins, C., De Propris, R., et al. 2005, MNRAS, 363, 661
Jedrzejewski, R. I. 1987, MNRAS, 226, 747
Jones, L. R., Ponman, T. J., Horton, A., et al. 2003, MNRAS, 343, 627
Kennicutt, R. C., Jr. 1992, ApJS, 79, 255
Khosroshahi, H. G., Jones, L. R., & Ponman, T. J. 2004, MNRAS, 349, 1240
Khosroshahi, H. G., Maughan, B. J., Ponman, T. J., & Jones, L. R. 2006, MNRAS, 369, 1211
Khosroshahi, H. G., Ponman, T. J., & Jones, L. R. 2007, MNRAS, 377, 595
La Barbera, F., de Carvalho, R. R., de la Rosa, I. G., et al. 2009, AJ, 137, 3942
Lidman, C., Iacobuta, G., Bauer, A. E., et al. 2013, MNRAS, 433, 825
Lieder, S., Mieske, S., Sánchez-Janssen, R., et al. 2013, A&A, 559, A76
Lin, Y.-T., & Mohr, J. J. 2004, ApJ, 617, 879
Mahdavi, A., & Geller, M. J. 2001, ApJ, 554, L129
Malumuth, E. M., Kriss, G. A., Dixon, W. V. D., Ferguson, H. C., & Ritchie, C. 1992, AJ, 104, 495
Materne, J. 1979, A&A, 74, 235
Mendes de Oliveira, C. L., Cypriano, E. S., & Sodré, L., Jr. 2006, AJ, 131, 158
Mendes de Oliveira, C. L., Cypriano, E. S., Dupke, R. A., & Sodré, L., Jr. 2009, AJ, 138, 502
Méndez-Abreu, J., Aguerri, J. A. L., Barrena, R., et al. 2012, A&A, 537, A25
Mukai, K. 1993, Legacy, 3, 21
Mulchaey, J. S., & Zabludoff, A. I. 1998, ApJ, 496, 73
Mulchaey, J. S., & Zabludoff, A. I. 1999, ApJ, 514, 133
Ortiz-Gil, A., Guzzo, L., Schuecker, P., Böhringer, H., & Collins, C. A. 2004, MNRAS, 348, 325
Pisani, A. 1996, MNRAS, 278, 697
Ponman, T. J., Allan, D. J., Jones, L. R., et al. 1994, Nature, 369, 462
Proctor, R. N., de Oliveira, C. M., Dupke, R., et al. 2011, MNRAS, 418, 2054
Quintana, H., & Melnick, J. 1982, AJ, 87, 972
Quintana, H., Carrasco, E. R., & Reisenegger, A. 2000, AJ, 120, 511
Santos, W. A., Mendes de Oliveira, C., & Sodré, L., Jr. 2007, AJ, 134, 1551
Shen, S., Yang, X., Mo, H., van den Bosch, F., & More, S. 2014, ApJ, 782, 23
Sommer-Larsen, J. 2006, MNRAS, 369, 958
Sun, M., Forman, W., Vikhlinin, A., et al. 2004, ApJ, 612, 805
The, L. S., & White, S. D. M. 1986, AJ, 92, 1248
Tonry, J., & Davis, M. 1979, AJ, 84, 1511
Voevodkin, A., Borozdin, K., Heitmann, K., et al. 2010, ApJ, 708, 1376
Voges, W., Aschenbach, B., Boller, T., et al. 1999, A&A, 349, 389
Voges, W., Aschenbach, B., Boller, T., et al. 2000, IAU Circ., 7432, 1
von Benda-Beckmann, A. M., D'Onghia, E., Gottlöber, S., et al. 2008, MNRAS, 386, 2345
Xue, Y.-J., & Wu, X.-P. 2000, ApJ, 538, 65
Zibetti, S., Pierini, D., & Pratt, G. W. 2009, MNRAS, 392, 525